Eur. Phys. J. C 22, 303–315 (2001)
Digital Object Identifier (DOI) 10.1007/s100520100797

THE EUROPEAN PHYSICAL JOURNAL C

# Is a large intrinsic $k_{\mathrm{T}}$ needed to describe photon + jet photoproduction at HERA?

M. Fontannaz[1], J.Ph. Guillet[2], G. Heinrich[1]

[1] Laboratoire de Physique Théorique LPT[a], Université de Paris XI, Bâtiment 210, 91405 Orsay, France
[2] Laboratoire d'Annecy-Le-Vieux de Physique Théorique LAPTH[b], Chemin de Bellevue, B.P. 110, 74941 Annecy-le-Vieux, France

Received: 1 August 2001 / Revised version: 18 September 2001 /
Published online: 21 November 2001 – 

**Abstract.** We study the photoproduction of an isolated photon and a jet based on a code of partonic event generator type which includes the full set of next-to-leading order corrections. We compare our results to a recent ZEUS analysis in which an effective $k_{\mathrm{T}}$ of the incoming partons has been determined. We find that no additional intrinsic $k_{\mathrm{T}}$ is needed to describe the data.

## 1 Introduction

Inclusive photoproduction of an isolated prompt photon has been measured at HERA [1] and compared to theoretical predictions [2–4] recently. The photoproduction of an isolated prompt photon and a jet was originally studied less extensively [5], and only partial next-to-leading order codes were available up to now [6,3]. However, the presence of the jet allows the definition of observables to be made which may provide a more detailed picture of the underlying partonic processes than in the inclusive case. In particular, it allows one to extract information on the transverse momentum $k_{\mathrm{T}}$ of the initial state partons.

The introduction of an effective initial state transverse momentum $\langle k_{\mathrm{T}}\rangle$ [7] has become a common practice in recent years [8–10] and has served to bridge large gaps between certain data and NLO theory in fixed target and hadronic collision experiments of prompt photon production. It has been argued that, in addition to the "intrinsic" transverse momentum of the initial state partons of a few hundred MeV due to the finite size of the proton, initial state soft gluon radiation can generate sizable transverse components of the parton momenta. Considerable progress has been made in recent times to account for multiple soft gluon emission effects in resummation formalisms [11–14], but the phenomenological application of such calculations has not reached a mature state yet. Therefore, simplified phenomenological models for $k_{\mathrm{T}}$ effects have been employed which introduce a Gaussian smearing of the parton transverse momenta, the mean value of this effective $k_{\mathrm{T}}$ being fitted from the data. However, these procedures are rather ad hoc, and various experiments lead to quite different conclusions [15,16] on the necessity to introduce an effective $k_{\mathrm{T}}$.

Recently, the ZEUS collaboration reported on the analysis of prompt photon plus jet photoproduction data with improved statistics [20]. From the comparison of the data to results obtained with the Monte Carlo program PYTHIA [21], it has been concluded in [20] that a total effective $\langle k_{\mathrm{T}}\rangle$ value of about 1.7 GeV is necessary to fit the data. This value is composed of the mean value of the intrinsic parton momentum in the proton, $\langle k_{\mathrm{T}}^{\mathrm{intr}}\rangle$, and the parton shower contribution to $\langle k_{\mathrm{T}}\rangle$. The two contributions are combined assuming that the overall distribution is Gaussian. The parton shower contribution was found to be approximately 1.4 GeV, and for $\langle k_{\mathrm{T}}^{\mathrm{intr}}\rangle$ a value of $\langle k_{\mathrm{T}}^{\mathrm{intr}}\rangle \approx 1.25$ GeV has been fitted. However, it was found that the same data are already well described by HERWIG [22] with a default parton intrinsic transverse momentum of zero.

In this paper, we compare NLO QCD results to the data presented in [20] and discuss in detail possible sources of differences between theory and data. In particular, we address the question whether an extra effective transverse momentum $\langle k_{\mathrm{T}}\rangle$ – in addition to the one already contained in fixed order NLO QCD – is necessary to fit the ZEUS data. We found that our NLO QCD prediction for the quantities which served to determine $\langle k_{\mathrm{T}}\rangle$ in [20] describes the data without taking into account any extra $k_{\mathrm{T}}$ effects. We recall that for single-inclusive prompt photon and $\pi^0$ data from fixed target and ISR experiments the situation is less evident, but as shown in [15], choosing the scales between $p_{\mathrm{T}}/2$ and $p_{\mathrm{T}}/3$ leads to agreement between NLO theory and data above $p_{\mathrm{T}} \approx 5$ GeV (below perturbative predictions become unstable) for all fixed target and ISR prompt photon data except the ones from the E706 experiment. For single-inclusive $\pi^0$ data, the

[a] Unité Mixte de Recherche 8627 du CNRS
[b] Unité Mixte de Recherche 5108 du CNRS, associée à l'Université de Savoie

shape of the $p_T$ spectrum is well described for all experiments, but the data lie systematically above the theory prediction, the difference in normalization being in average about 50% [16]. The NLO calculation had been done with a set of fragmentation functions [17] which has been updated meanwhile. Redoing the analysis with the most recent set of fragmentation functions [18] leads to agreement between theory and data for $p_T$ values larger than about 5 GeV [19].

Our results have been obtained with a program of partonic event generator type which includes the full next-to-leading order corrections to all the partonic subprocesses, as well as the box contribution $\gamma g \to \gamma g$. The program already has been used to study inclusive prompt photon photoproduction [4], and has been extended to allow also the calculation of prompt photon plus jet photoproduction in the present work.

This paper is organized as follows. In Sect. 2, we first describe the main lines of the calculation our code is based on. Then we discuss the effect of certain kinematic cuts and infrared sensitive limits which will be relevant for the comparison to the ZEUS data. In Sect. 3 we give numerical results for the isolated photon plus jet cross-section and compare to the ZEUS data. Section 4 contains the study of $k_T$-sensitive observables. We show our results for the $p_\perp$ and $\Delta\phi$ distributions used by ZEUS to determine $\langle k_T \rangle$ and discuss their implications. An appendix contains details of the discussion of symmetric cuts contained in Sect. 2.

## 2 Description of the method

### 2.1 General setting

As the general framework of the calculation already has been described in detail in [4], we will give only a brief overview on the method here.

In photoproduction events, the electron acts like a source of quasi-real photons whose spectrum can be described by the Weizsäcker–Williams formula

$$f_\gamma^e(y) = \frac{\alpha_{\rm em}}{2\pi}\left\{\frac{1+(1-y)^2}{y}\ln\frac{Q^2_{\max}(1-y)}{m_e^2 y^2} - \frac{2(1-y)}{y}\right\}. \quad (1)$$

The quasi-real photon then either takes part *directly* in the hard scattering process, or it acts as a composite object, being a source of partons which take part in the hard subprocess. The latter mechanism is referred to as a *resolved* process and is parameterized by the photon structure functions $F_{a/\gamma}(x_\gamma, Q^2)$. Thus the distribution of partons in the electron is a convolution

$$F_{a/e}(x_e, M) = \int_0^1 {\rm d}y{\rm d}x_\gamma f_\gamma^e(y) F_{a/\gamma}(x_\gamma, M)\delta(x_\gamma y - x_e), \quad (2)$$

where in the "direct" case $F_{a/\gamma}(x_\gamma, M) = \delta_{a\gamma}\delta(1-x_\gamma)$.

Similarly, a high-$p_T$ photon in the final state can either originate directly from the hard scattering process or it can be produced by the fragmentation of a hard parton emerging from the hard scattering process. Thus we distinguish four categories of production mechanisms, as illustrated in Fig. 1:

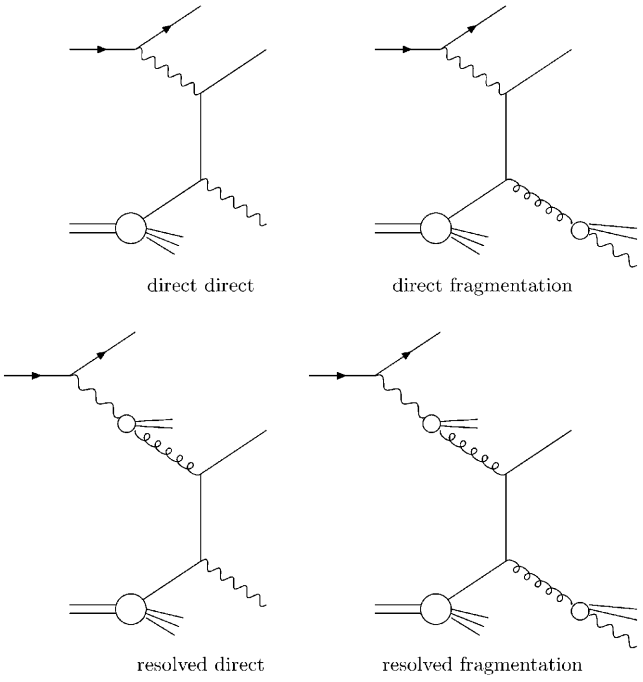


**Fig. 1.** Examples of contributing subprocesses at leading order

(1) direct direct;
(2) direct fragmentation;
(3) resolved direct;
(4) resolved fragmentation.

We implemented the full set of next-to-leading order corrections to all four subprocesses. Note that the photon structure functions behave for large $Q^2$ as $F_{a/\gamma}(x, Q^2) \sim \ln Q^2/\Lambda^2 \sim 1/\alpha_s(Q^2)$. An analogous argument holds for the fragmentation functions, such that a consistent NLO calculation requires the inclusion of the full $\mathcal{O}(\alpha_s)$ corrections not only to the "direct direct" part but also to the resolved and/or fragmentation parts[1]. The matrix elements for these NLO corrections have been taken from the literature [24–26]. We also included the box contribution $g\gamma \to g\gamma$, which is NNLO if one just counts the powers of $\alpha_s$. However, as already pointed out some time ago [27,28], its contribution is sizable, the order of magnitude being about 20% of the Born cross-section in our present numerical study. The box contributions to the resolved/fragmentation parts are suppressed with respect to $g\gamma \to g\gamma$ by at least a factor 10 coming from charge and colour factors. The box contribution $g\gamma \to g\gamma$ is conceptually different from the whole set of NNLO corrections since it is not a higher order correction to a process which already exists at Born level, but an additional $2 \to$

[1] In the following, we will denote by "resolved" the sum of resolved direct and resolved fragmentation parts and by "direct" the sum of direct direct and direct fragmentation parts

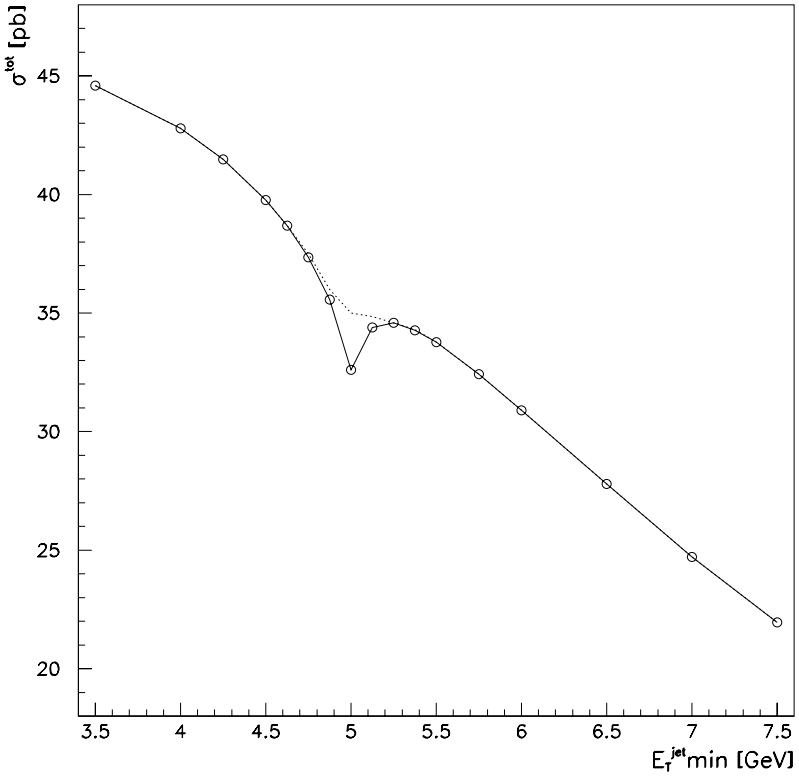


**Fig. 2.** Non-isolated total $\gamma+$ jet cross-section for $E_{\rm T}^{\gamma} > 5\,\text{GeV}$ as a function of $E_{\rm T,min}^{\rm jet}$. The photon energy range is $0.2 < y < 0.9$, the rapidities are integrated over $-1.5 < \eta^{\rm jet} < 1.8$ and $-0.7 < \eta^{\gamma} < 0.9$

2 subprocess which can enter only through a fermion loop. The "regular" NNLO corrections to the direct direct part, which are formally of the same order in $\alpha_{\rm s}$ as the box contribution, are not included here since they are expected to be much smaller than the direct direct Born term (if one does not question the validity of perturbation theory), such that it is unlikely that they will conspire to cancel the contribution from the $g\gamma \to g\gamma$ process.

It is well known that at NLO the attribution of certain finite terms to either of the four categories listed above is scheme dependent and therefore only the sum of all parts has a physical meaning.

In order to isolate the infrared singularities appearing in the calculation at next-to-leading order, a modified phase-space slicing method has been used [4,23].

For the definition of jets, the $k_{\rm T}$ algorithm of [29] has been employed, as has been done by the ZEUS collaboration.

To single out the prompt photon events from the background of secondary photons produced by the decays of light mesons, isolation cuts have to be imposed on the photon signals in the experiment. We use the following isolation criterion: In a cone $C$ centered around the photon direction in the rapidity and azimuthal angle plane, defined by

$$C = \left\{(\eta,\phi)|\,(\eta-\eta_\gamma)^2 + (\phi-\phi_\gamma)^2 \le R^2\right\},$$

the amount of deposited hadronic transverse energy $E_{\rm T}^{\rm had}$ ($R$) is required to be smaller than a fraction $\epsilon_{\rm c}$ of the photon transverse momentum. We use $\epsilon_{\rm c} = 0.1$ and $R = 1$ to match the cuts of the ZEUS collaboration.

Since isolation cuts impose additional phase-space restrictions, the question has been raised if factorization properties valid for the inclusive case might be spoiled by isolation. This issue is discussed in detail in [34,35]. Here we just note that the above criterion, being based on boost-invariant *transverse* energies, leads to infrared safe cross-sections.

## 2.2 Effects of kinematic cuts, infrared sensitive limits

As a consequence of phase-space restrictions induced for example by kinematic cuts, certain observables calculated at fixed order may show instabilities (integrable singularities) at some critical point of phase space [33,34]. Examples will be discussed below.

### 2.2.1 Symmetric cuts on $E_{\rm T}^{\rm jet}, E_{\rm T}^{\gamma}$

In order to restrict both prompt photons and jets to well-measured kinematic regions, the ZEUS collaboration has required $E_{\rm T}^{\gamma} > 5\,\text{GeV}$ and $E_{\rm T}^{\rm jet} > 5\,\text{GeV}$ in their analysis [20]. However, as is well known [36,37], symmetric cuts on the transverse energies should be avoided since they select a region where fixed order NLO QCD loses its predictive power. This can be seen by considering the total cross-section as a function of $E_{\rm T,min}^{\rm jet}$ as shown in Fig. 2. The cut on the transverse energy of the photon has been fixed to $E_{\rm T,min}^{\gamma} = 5\,\text{GeV}$. The figure shows that the NLO QCD prediction varies rapidly around the point $E_{\rm T,min}^{\rm jet} = E_{\rm T,min}^{\gamma}$.

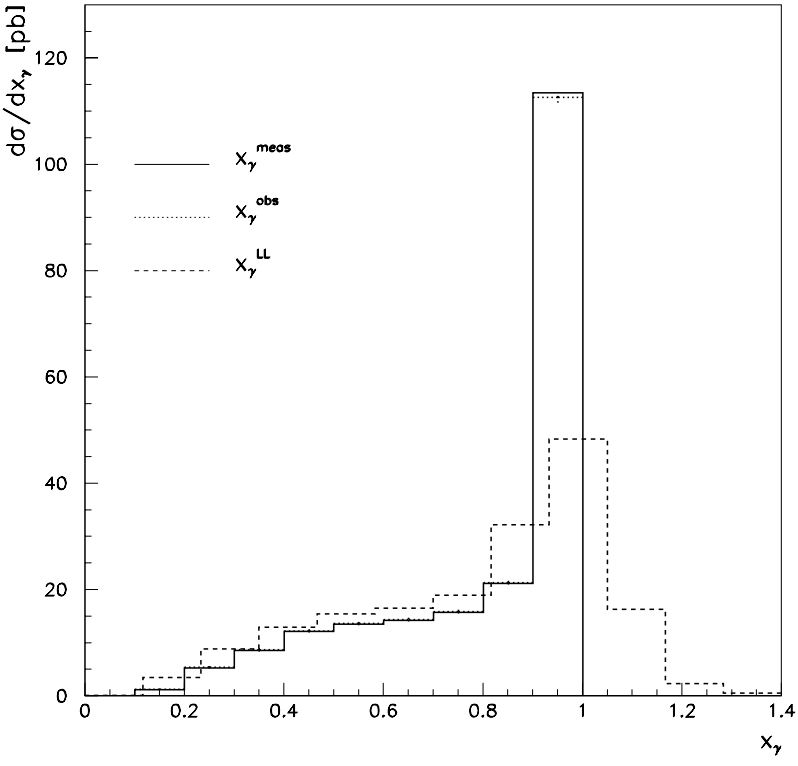


**Fig. 3.** Behavior of $\mathrm{d}\sigma/\mathrm{d}x_\gamma^{\mathrm{LL}}$, $\mathrm{d}\sigma/\mathrm{d}x_\gamma^{\mathrm{meas}}$ and $\mathrm{d}\sigma/\mathrm{d}x_\gamma^{\mathrm{obs}}$ for the isolated $\gamma$ + jet cross-section

In particular, it is striking that the cross-section is *not* immediately monotonically decreasing for increasing $E_{\mathrm{T,min}}^{\mathrm{jet}}$. The reason for the dip at $E_{\mathrm{T,min}}^{\mathrm{jet}} = E_{\mathrm{T,min}}^{\gamma}$ is that at this point the phase space for the unobserved parton in the real corrections is severely restricted, such that the (negative) virtual corrections are not sufficiently balanced by the (positive) real corrections[2]. As a result we observe a violation of unitarity in the range $5.0\,\mathrm{GeV} \leq E_{\mathrm{T,min}}^{\mathrm{jet}} \leq 5.25\,\mathrm{GeV}$, where the cross-section increases when the available phase space decreases. This phenomenon, that we discuss in detail in the appendix, is an artifact of the fixed order calculation. In this particular region around $E_{\mathrm{T,min}}^{\mathrm{jet}} = E_{\mathrm{T,min}}^{\gamma}$, the higher order corrections should be resummed to produce a curve that should look like the dashed curve in Fig. 2. This resummation is not considered in this paper (but the large logarithms responsible for this behavior are identified, see Appendix A) because the unphysical effect at $E_{\mathrm{T,min}}^{\mathrm{jet}} = E_{\mathrm{T,min}}^{\gamma}$ is in general numerically weak. However, we shall explore the effect of different choices of $E_{\mathrm{T,min}}^{\mathrm{jet}}$ when calculating the cross-section corresponding to the ZEUS data. It is clear that an asymmetric cut in the experiment would avoid any trouble.

### 2.2.2 Definition of $x_\gamma$, limit $x_\gamma \to 1$

Care also has to be taken in the treatment of the variable $x_\gamma$ near the boundary $x_\gamma \to 1$. At leading order, the fraction $x_\gamma$ of the incoming photon longitudinal momentum is defined as

$$x_\gamma = \frac{E_{\mathrm{T3}}(\mathrm{e}^{-\eta_3} + \mathrm{e}^{-\eta_4})}{2E_\gamma} \tag{3}$$

where $\eta_3$ and $\eta_4$ are the rapidities of the two outgoing partons and $E_\gamma = yE_e$. At next-to-leading order, the "true" $x_\gamma$ for $2 \to 3$ processes is given by $x_\gamma = \sum_{i=3}^{5}(E_{\mathrm{T}i}\mathrm{e}^{-\eta_i})/(2E_\gamma)$, but since particle 5 is not observed, $x_\gamma$ is no longer an experimentally accessible observable. Hence, to obtain an estimate of the longitudinal momentum fraction of the incoming photon, the variable $x_\gamma^{\mathrm{obs}}$, defined as

$$x_\gamma^{\mathrm{obs}} = \frac{E_{\mathrm{T}}^{\gamma}\mathrm{e}^{-\eta^\gamma} + E_{\mathrm{T}}^{\mathrm{jet}}\mathrm{e}^{-\eta^{\mathrm{jet}}}}{2E_\gamma} \tag{4}$$

is frequently used. However, the above definition of $x_\gamma^{\mathrm{obs}}$ may lead to infrared sensitive cross-sections [38]. Fixing $E_{\mathrm{T}}^{\gamma}$ *and* $E_{\mathrm{T}}^{\mathrm{jet}}$ strongly constrains the phase space of parton 5 when $x_\gamma^{\mathrm{obs}}$ goes to 1. This is reflected by $\log(1 - x_\gamma^{\mathrm{obs}})$ terms generated by the higher order corrections. In general, $x_\gamma^{\mathrm{obs}}$ is integrated over, typically in the range $0.75 \leq x_\gamma^{\mathrm{obs}} \leq 1$, such that the singular behavior is sufficiently smoothed out for a fixed order calculation to remain valid. However, if the width of the last bin at $x_\gamma^{\mathrm{obs}} \to 1$ is small, the shape of the theoretical prediction near $x_\gamma^{\mathrm{obs}} = 1$ is considerably dependent on the bin width. For this reason, the variable $x_\gamma^{\mathrm{LL}} = E_{\mathrm{T}}^{\gamma}(\mathrm{e}^{-\eta^\gamma} + \mathrm{e}^{-\eta^{\mathrm{jet}}})/(2E_\gamma)$, which has a smoother behavior for $x_\gamma \to 1$, has been proposed in [38]. It also has the advantage that it does not depend on $E_{\mathrm{T}}^{\mathrm{jet}}$ and thus does not contain an uncertainty from the jet en-

[2] We checked by varying the phase-space slicing parameter that this effect is not an artifact of the slicing method

ergy reconstruction. Note that $x_\gamma^{\rm LL}$ can be bigger than 1, as illustrated in Fig. 3.

For the analysis presented in [20], the ZEUS collaboration did not use $x_\gamma^{\rm obs}$, but the variable $x_\gamma^{\rm meas}$, defined as

$$x_\gamma^{\rm meas} = \frac{\sum_{\gamma,i}(E-p_z)}{2E_e y^{\rm JB}} = \frac{E_{\rm T}^\gamma {\rm e}^{-\eta^\gamma} + \sum_i E_{{\rm T}i}{\rm e}^{-\eta^i}}{2E_e y^{\rm JB}}, \quad (5)$$

where the sum is over the prompt photon and the contents of the jet, and $y^{\rm JB}$ is the energy fraction of the incoming photon, reconstructed with the Jacquet–Blondel method:

$$y^{\rm JB} = \frac{\sum(E-p_z)}{2E_e}. \quad (6)$$

Here the sum is over all energy-flow objects in the event, each of which is treated as due to a massless particle with energy $E$ and longitudinal momentum component $p_z$. From an experimental point of view, $x_\gamma^{\rm meas}$ is convenient since a lot of calorimeter calibration systematics cancel out. The difference between definitions (4) and (5) for $x_\gamma$ depends on the definitions of $E_{\rm T}^{\rm jet}$ and $\eta^{\rm jet}$ in (4). If the Snowmass conventions

$$E_{\rm T}^{\rm jet} = \sum_i E_{{\rm T}i}, \quad \eta^{\rm jet} = \frac{\sum_i E_{{\rm T}i}\eta^i}{E_{\rm T}^{\rm jet}}, \quad \phi^{\rm jet} = \frac{\sum_i E_{{\rm T}i}\phi^i}{E_{\rm T}^{\rm jet}} \quad (7)$$

are used, one has

$$\begin{aligned} x_\gamma^{\rm meas} - x_\gamma^{\rm obs} &= \frac{1}{2E_\gamma}\left\{\sum_i E_{{\rm T}i}{\rm e}^{-\eta^i} - \left(\sum_i E_{{\rm T}i}\right){\rm e}^{-(\sum_i E_{{\rm T}i}\eta_i)/E_{\rm T}^{\rm jet}}\right\} \\ &\geq 0. \end{aligned}$$

For our analysis, where maximally two massless partons form a jet, the difference between $x_\gamma^{\rm obs}$ and $x_\gamma^{\rm meas}$ is numerically indistinguishable (see Fig. 3).

Obviously, what has been said above on the limit $x_\gamma^{\rm obs} \to 1$ is valid for $x_\gamma^{\rm meas} \to 1$ as well.

## 3 Numerical results and comparison to ZEUS data

For the numerical studies we use the rapidity cuts $-1.5 < \eta^{\rm jet} < 1.8$ and $-0.7 < \eta^\gamma < 0.9$ chosen by ZEUS to restrict the photon and the jet to well-measured kinematic regions. We also use the cuts $E_{\rm T,min}^{\rm jet} = E_{\rm T,min}^\gamma = 5\,{\rm GeV}$ in order to match the ZEUS cuts, although such symmetric cuts select a region where fixed order perturbative QCD shows instabilities, as discussed in detail in Sect. 2.2 and in the appendix. From Fig. 2 one can estimate that the uncertainty in the theoretical prediction introduced by using these cuts is of the order of 6–10% for the total cross-section.

We set $Q^2_{\rm max} = 1\,{\rm GeV}^2$ for the virtuality of the photons in (1) and restrict the photon energy to the range $0.2 < y < 0.7$ as reconstructed by ZEUS. We take the MRST2 [30] parameterization for the parton distributions in the proton, AFG [31] for the parton distributions in the photon, BFG [32] for the fragmentation functions into photons, $n_f = 4$ flavors, and for $\alpha_{\rm s}(\mu)$ we use an exact solution of the two-loop renormalization group equation, and not an expansion in $\log(\mu/\Lambda)$. Unless stated otherwise, the scale choice $\mu = p_{\rm T}^\gamma$ has been adopted and $M$ and $M_F$ have been set equal to $\mu$. The rapidities refer to the $ep$ laboratory frame, with the HERA convention that the proton is moving towards positive rapidity.

Figure 4 shows the relative magnitude of the NLO result to the leading order[3] result for the isolated-photon rapidity distribution. As the box contribution has the same kinematics as the leading order direct direct part, we included the box contribution in this part, such that "direct direct" always means direct direct plus box. Since the higher order corrections to the direct direct term are negative and those to the resolved part are small (for the scale choice $\mu = p_{\rm T}^\gamma$, see Fig. 5), the overall NLO result is lower than the leading order result. We note that the higher order corrections to the direct part are most negative for $E_{\rm T,min}^{\rm jet} = E_{\rm T,min}^\gamma$, for asymmetric cuts the absolute value of the negative contributions decreases.

In order to single out the events stemming from a direct photon in the initial state, the cut $x_\gamma^{\rm meas} > 0.9$ has been applied by ZEUS. However, it has to be kept in mind that beyond leading order, the direct part has a non-negligible tail away from $x_\gamma^{\rm meas} = 1$, and that the contributions from the resolved part to the bin $x_\gamma^{\rm meas} > 0.9$ are rather large, as can be seen from Fig. 6a. Figure 6b compares the sum direct + resolved with the cut $x_\gamma^{\rm meas} > 0.9\,(0.85)$ to direct direct only with no cut on $x_\gamma^{\rm meas}$ for the photon rapidity distribution. One observes that there is a significant difference in the shape between the direct part and the result obtained by imposing the cut $x_\gamma^{\rm meas} > 0.9$ to the full set of subprocesses, the latter being higher in the backward region and lower in the forward region. Hence imposing a stringent cut on $x_\gamma^{\rm meas}$ cannot be considered as fully equivalent to singling out the direct events only.

### 3.1 Comparison of photon rapidity and $x_\gamma$ distributions to ZEUS data

Figure 7 shows the distributions ${\rm d}\sigma/{\rm d}x_\gamma^{\rm meas}$ and the photon rapidity distribution for various scale choices together with the ZEUS data. One can see that the theoretical uncertainty due to overall scale variations, i.e. varying $\mu$ between $p_{\rm T}^\gamma/2$ and $2p_{\rm T}^\gamma$ and setting $M_F = M = \mu$, is very small. For the distribution in $x_\gamma^{\rm meas}$ one observes that the theory overshoots the data substantially in the last bin, whereas the data are described well in the remaining bins. In ${\rm d}\sigma/{\rm d}\eta^\gamma$ there is a rather large discrepancy between theory and data in the forward region.

[3] By "leading order" we mean the sum of the lowest order terms of all four subprocesses direct direct, direct fragmentation, resolved direct and resolved fragmentation

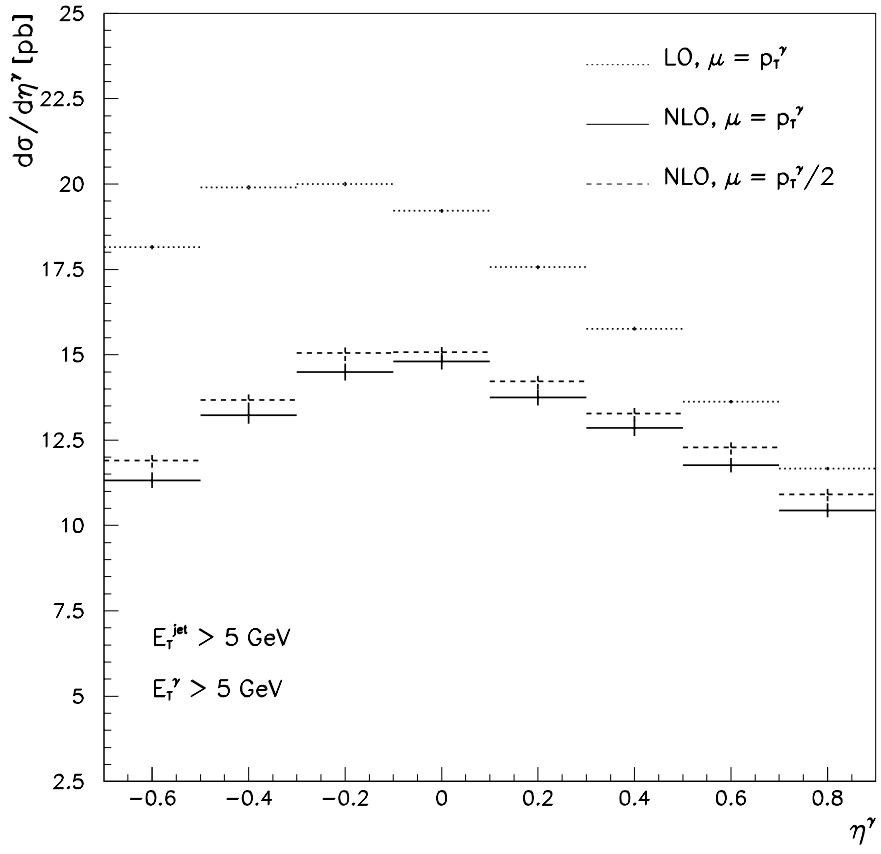


**Fig. 4.** Magnitude of leading order and NLO results for the isolated cross-section $\mathrm{d}\sigma^{\gamma+\mathrm{jet}}/\mathrm{d}\eta^{\gamma}$. Isolation with $\epsilon_{\rm c} = 0.1, R = 1$, jet rapidities integrated over $-1.5 < \eta^{\rm jet} < 1.8$

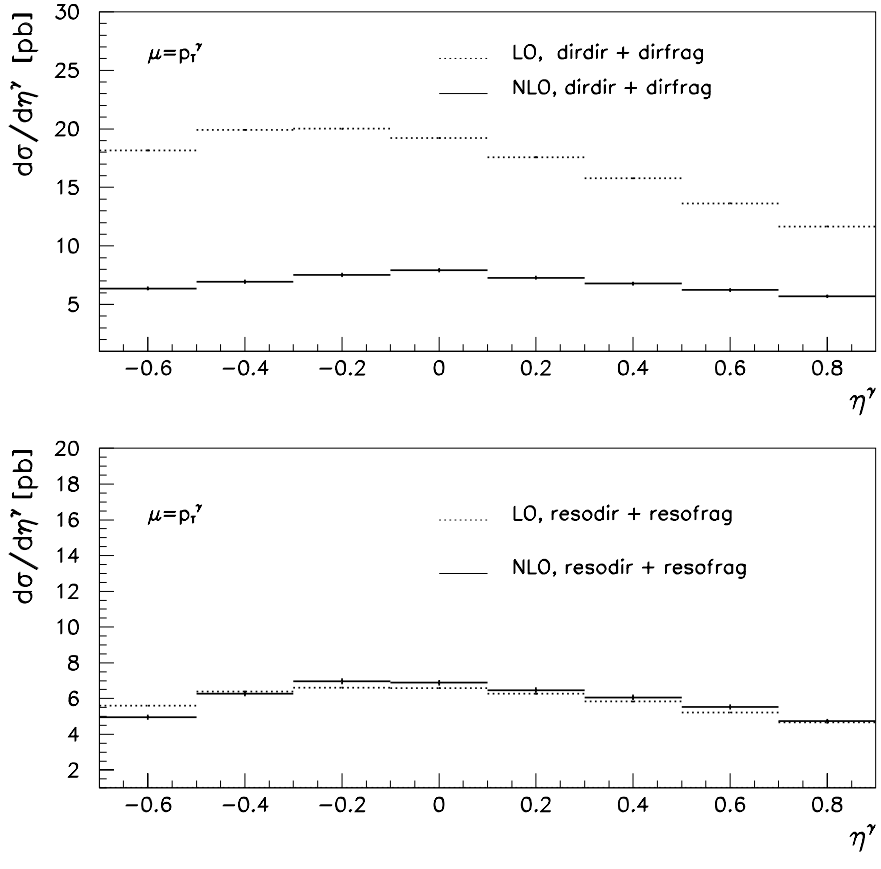


**Fig. 5.** Magnitude of LO and NLO contributions for resolved and direct parts separately, with isolation ($\epsilon_{\rm c} = 0.1, R = 1$)

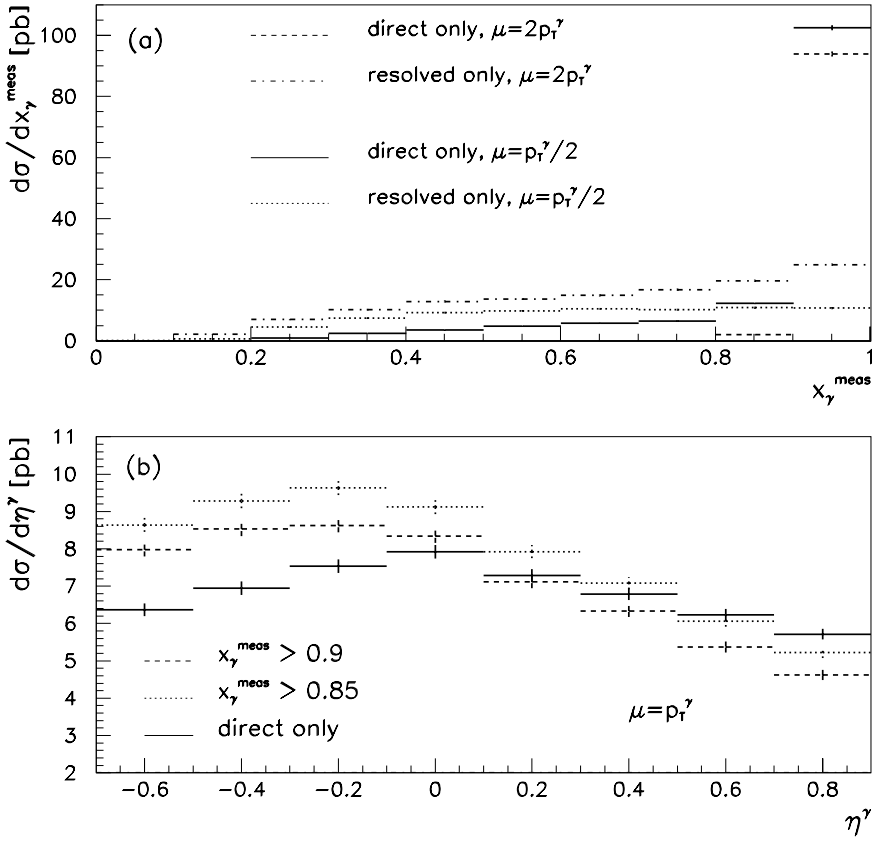


**Fig. 6. a** $d\sigma/dx_\gamma^{meas}$ for direct and resolved components separately and two different scale choices, **b** $d\sigma/d\eta^\gamma$ for direct component (no cut) compared to the full result with the cut $x_\gamma^{meas} > 0.9\,(0.85)$

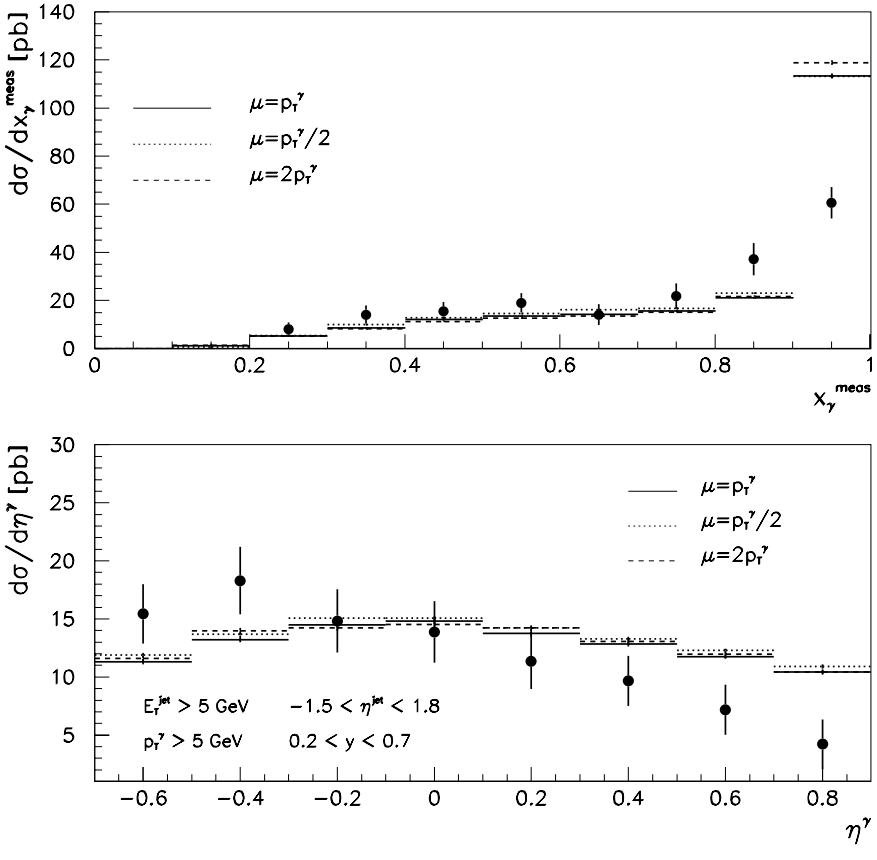


**Fig. 7.** $d\sigma^{\gamma+jet}/dx_\gamma^{meas}$ and $d\sigma^{\gamma+jet}/d\eta^\gamma$ for the scale choices $\mu = p_T^\gamma$ (default), $\mu = p_T^\gamma/2$ and $\mu = 2p_T^\gamma$ (always $M_F = M = \mu$) together with the ZEUS data. The errors on the data are statistical only

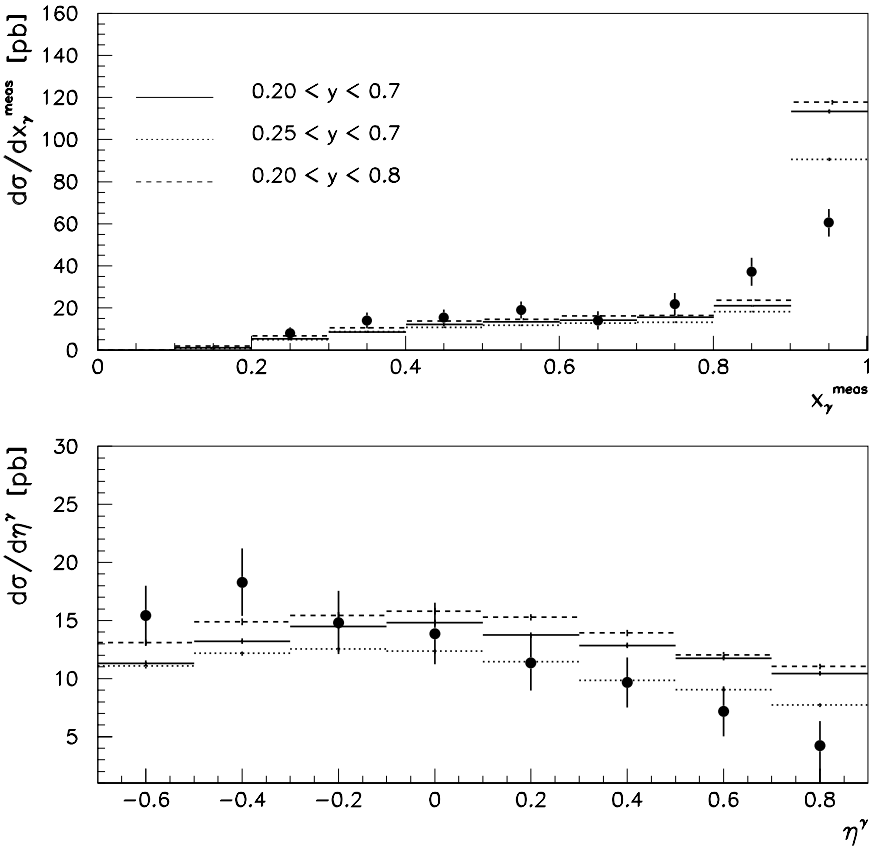


**Fig. 8.** $d\sigma^{\gamma+\text{jet}}/dx_\gamma^{\text{meas}}$ and photon rapidity distribution $d\sigma^{\gamma+\text{jet}}/d\eta^\gamma$ for different cuts on the photon energy: $0.2 < y < 0.7$ (default), $0.25 < y < 0.7$, $0.2 < y < 0.8$

The reasons for these discrepancies may be the following.

(1) The data are at the detector level, i.e. they are not fully corrected for energy losses in the detector and other effects. Therefore data corrected to the hadron level may differ in a non-negligible way from the ones displayed in Fig. 7. For example, it is possible that the efficiency of event detection is less at high rapidity, such that the data for the rapidity distribution would be higher in the forward region after correction for detector effects. Moreover our calculations are performed at the parton level and hadronization effects may also lead to sizable corrections at these low values of $p_T^{\text{jet}}$ (see also point (4) below).

(2) There is an uncertainty in the reconstruction of the "true" photon energy $y$ with the Jacquet–Blondel method (cf. (6)). In general, corrections for detector effects and energy calibration tend to shift the range of $y$ to slightly higher values as compared to the original range of $y^{\text{JB}}$. To study the effect of an uncertainty in $y$, we varied the cuts on $y$, increasing the lower cut from $y_{\min} = 0.2$ to $y_{\min} = 0.25$, respectively increasing the upper cut from $y_{\max} = 0.7$ to $y_{\max} = 0.8$, as shown in Fig. 8.

(3) Concerning $d\sigma/dx_\gamma^{\text{meas}}$, we can make the following remark. There is an uncertainty in the energy and $p_z$ values entering in the definition (5) of $x_\gamma^{\text{meas}}$. Taking into account this uncertainty in the calculation would introduce a Gaussian smearing in $E$ and $p_z$ which would smooth out the theoretical curve near $x_\gamma^{\text{meas}} \to 1$.

(4) As already discussed in [4], a non-negligible part of the hadronic energy measured in the isolation cone may be due to underlying events, especially in the forward region. Therefore it is possible that experimentally, the isolation cut removes events which pass in the theoretical (parton level) simulation since there the underlying event contamination is not present. It has been estimated [4] that this can have an effect of the order of 30% in the forward region.

Figure 9 again demonstrates (see also Fig. 2) that the cross-section is very sensitive to a variation of $E_{T,\min}^{\text{jet}}$ around the value $E_{T,\min}^{\text{jet}} = E_{T,\min}^{\gamma}$. It can be clearly seen that increasing the cut on $E_T^{\text{jet}}$ from 5 GeV to 5.5 GeV does *not* lead to a decrease in the cross-section, as explained in Sect. 2.2. For the rapidity distribution the theoretical uncertainty introduced by using symmetric cuts can be as large as 30%.

An intrinsic $\langle k_T \rangle$ would not improve the agreement between theory and data for the photon rapidity distribution, since it would shift the theoretical curve upwards without changing its shape. We note also that the data for $d\sigma/d\eta^\gamma$ and $d\sigma/dx_\gamma^{\text{meas}}$ are in general well described by PYTHIA 6.129 with default $\langle k_T \rangle$ values [20]. Only in the backward region in the photon rapidity distribution, PYTHIA is lower than the data; the same trend is visible in the NLO theory curve.

Figure 10 shows the contributions from direct and resolved initial state photons separately. As those parts sep-

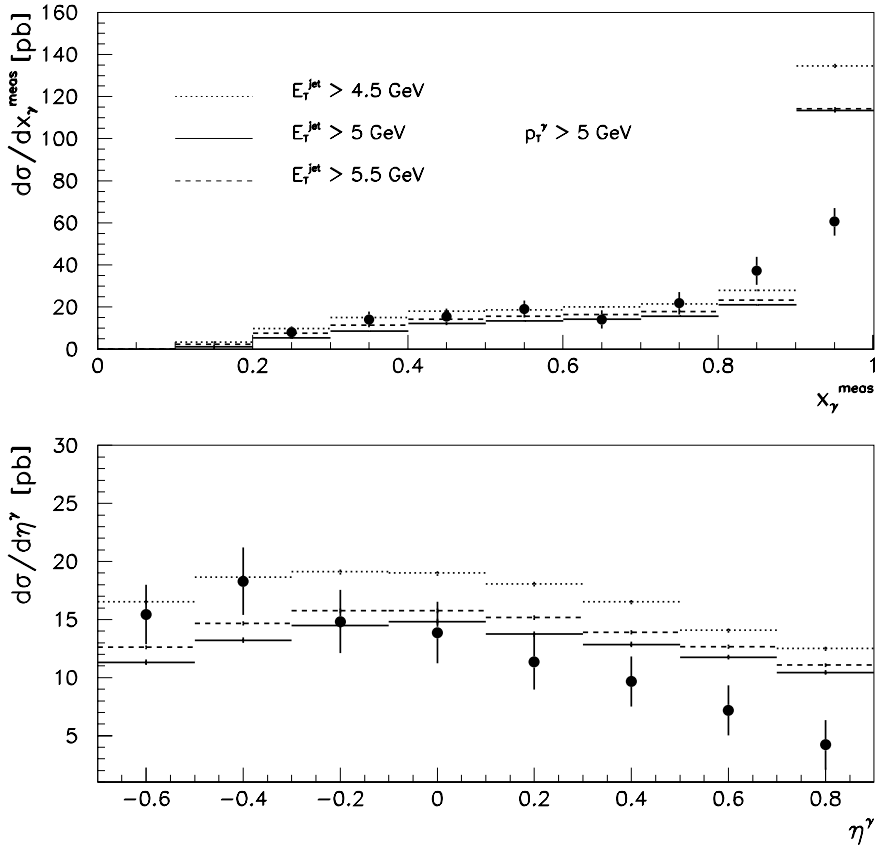


**Fig. 9.** $\mathrm{d}\sigma^{\gamma+\mathrm{jet}}/\mathrm{d}x_\gamma^{\mathrm{meas}}$ and $\mathrm{d}\sigma^{\gamma+\mathrm{jet}}/\mathrm{d}\eta^\gamma$ for different cuts on $E_{\mathrm{T}}^{\mathrm{jet}}$

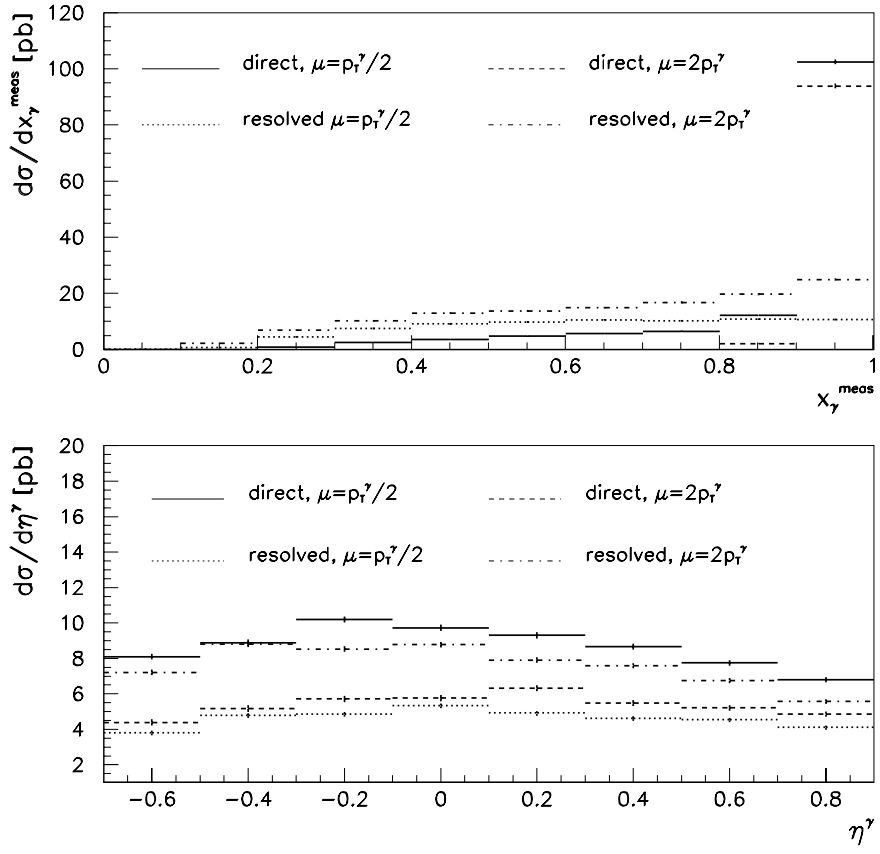


**Fig. 10.** Contributions from resolved and direct initial state photons separately for two different scale choices

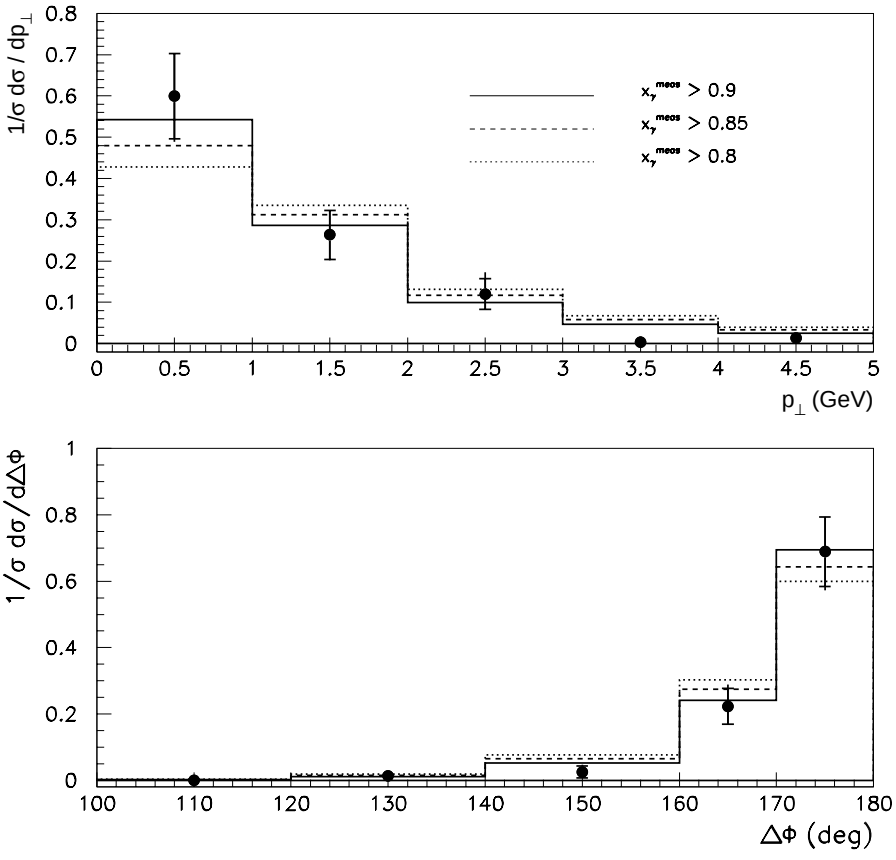


**Fig. 11.** Normalized cross-section differential in $p_\perp$ and $\Delta\phi$ for $x_\gamma^{\rm meas} > 0.8, 0.85, 0.9$. The inner error bars represent the statistical errors only, the outer bars represent the total uncertainty

arately are highly scale dependent, results for two ("extreme") scale choices are shown. The figure for the rapidity distribution illustrates that the statement which part – i.e. the resolved or direct part – dominates in the forward region, is scale dependent.

## 4 Results for $k_{\rm T}$-sensitive observables and comparison to ZEUS data

In this section we compare our results with the ZEUS data for the $k_{\rm T}$-sensitive observables $p_\perp$ and $\Delta\phi$ which served to determine $\langle k_{\rm T}\rangle$ in [20]. The quantity $p_\perp$ is the momentum component of the photon perpendicular to the jet direction, defined as

$$p_\perp = |\boldsymbol{p}_{\rm T}^{\gamma} \times \boldsymbol{p}_{\rm T}^{\rm jet}|/p_{\rm T}^{\rm jet}. \qquad (8)$$

Here $p_{\rm T}^{\rm jet}$ is *not* the Snowmass $E_{\rm T}^{\rm jet}$, but the modulus of the transverse components of the vector sum of the particle momenta which form the jet. $\Delta\phi$ is the azimuthal acollinearity between the photon and the jet. To define $\Delta\phi$, the Snowmass definition (see (7)) for the jet azimuthal angle has been used by ZEUS. In the experiment, a cut of $x_\gamma^{\rm meas} > 0.9$ has been imposed in order to select events which are predominantly from direct incoming photons, thereby suppressing eventual contributions to $\langle k_{\rm T}\rangle$ from the resolved photon. The data for these quantities have been corrected to hadron level. As the value of $\langle k_{\rm T}\rangle$ affects mainly the shape of the distributions, the cross-sections have been normalized to 1 in order to minimize uncertainties in the calorimeter energy scale.

Figure 11 shows the $p_\perp$ and $\Delta\phi$ distributions together with the ZEUS data. One can see that NLO QCD does describe the ZEUS data well without any intrinsic $k_{\rm T}$ or resummation taken into account. A reason for the fact that no need for resummation near $\Delta\phi = \pi$ or $p_\perp = 0$ is visible might be that the bin size is relatively large.

Since there is an uncertainty in the reconstruction of $x_\gamma^{\rm meas}$, we investigated the effect of shifting the cut on $x_\gamma^{\rm meas}$, as illustrated in Fig. 11. The reason why the result for the last bin $p_\perp \to 0$ respectively $\Delta\phi \to \pi$ decreases if the lower cut on $x_\gamma^{\rm meas}$ is decreased is related to the fact that for $x_\gamma^{\rm meas} > 0.8$ more inelastic processes contribute than for $x_\gamma^{\rm meas} > 0.9$, such that the ratio of nearly back-to-back events to the full cross-section decreases.

Note that we used symmetric cuts $E_{\rm T,min}^{\rm jet} = E_{\rm T,min}^{\gamma} = 5\,{\rm GeV}$ in order to match the ZEUS cuts. As discussed above, the theoretical result shows instabilities for symmetric cut values. Therefore we investigated the effect of varying $E_{\rm T,min}^{\rm jet}$ by 10% around the critical point $E_{\rm T,min}^{\gamma} = 5\,{\rm GeV}$, as shown in Fig. 12. One can see that the result varies by less than 10% in the normalized cross-sections. The effect of an uncertainty in the cuts on the photon energy $y$ has been found to be negligible in the area normalized plots.

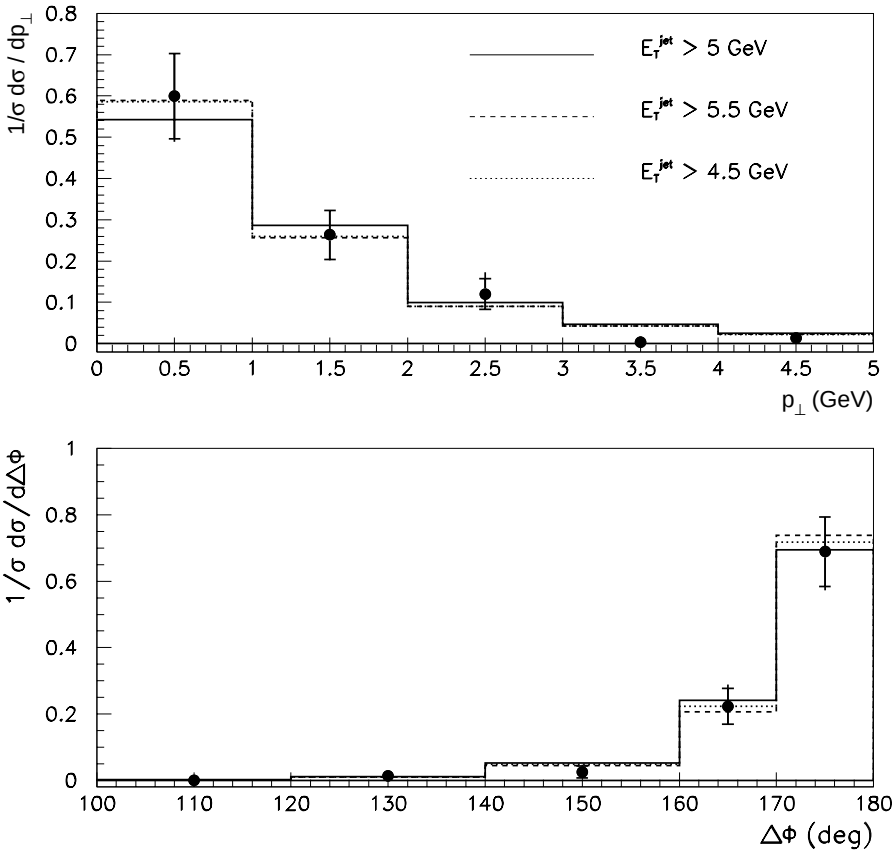


**Fig. 12.** Normalized cross-section differential in $p_\perp$ and $\Delta\phi$ for $E_{\mathrm{T,min}}^{\mathrm{jet}} = 4.5, 5$ and 5.5 GeV with $x_\gamma^{\mathrm{meas}} > 0.9$. The inner and outer error bars correspond to statistical and total errors, respectively

Hence we can say that the agreement between fixed order NLO QCD and data is very good in the case studied here. No $k_T$ in addition to the one already implicitly accounted for by including the full set of NLO corrections is needed. We recall that he same was true for the inclusive case [4], but of course there the sensitivity to $k_T$ is smaller.

Further we note that the *intrinsic* $k_T$ (i.e. the component of $\langle k_T \rangle$ that does not include the parton shower contribution) determined by the ZEUS collaboration to fit best the data has been obtained by comparing to simulations with PYTHIA 6.129. On the other hand, it was also found that the data are already well described by HERWIG 6.1 with the default parton $\langle k_T^{\mathrm{intr}} \rangle$ of zero [20]. The reason might stem from differences in the way the parton showering is implemented in HERWIG and PYTHIA. HERWIG does not use a sharp lower cut-off in the shower evolution below which PYTHIA relies on a suitable value of $\langle k_T^{\mathrm{intr}} \rangle$.

## 5 Conclusions

We have presented a full next-to-leading order calculation for the photoproduction of an isolated photon accompanied by a jet, based on a program of partonic event generator type.

We found that the variation of our result due to scale changes is very weak. We also investigated the sensitivity of the cross-section to variations of the photon energy, to different cuts on $x_\gamma$ and to the cut $E_{\mathrm{T,min}}^{\mathrm{jet}}$ on the jet transverse energy. In particular, we discussed in detail the instabilities arising at fixed order NLO QCD if symmetric cuts on the photon and jet transverse energies are chosen.

In comparing the $x_\gamma$ distribution to the ZEUS data we found that the agreement is good except near $x_\gamma \to 1$. For the photon rapidity distribution we found that our prediction is below the data in the backward region and overpredicts the data in the forward region. However, as the data for the $x_\gamma$ and rapidity distributions are at detector level, corrections for detector effects may change the situation. We discussed in detail possible sources of discrepancies between theory and data.

We also compared our results to recent ZEUS data for $k_T$-sensitive observables. Since the comparison has been done for normalized cross-sections, the effect of variations in the photon energy, $x_\gamma^{\mathrm{cut}}$ or $E_{\mathrm{T,min}}^{\mathrm{jet}}$ turned out to be very small. We found that NLO QCD already describes these data well without introduction of any additional intrinsic $k_T$.

Our results are in contrast to the results found in the E706 fixed target experiment [9], where the conclusion was that high-$p_T$ prompt photon and $\pi^0$ data could not be well described by NLO perturbative QCD without the incorporation of substantial extra $k_T$ effects.

*Acknowledgements.* We are grateful to P. Bussey from the ZEUS collaboration for helpful discussions. G.H. would like to

thank the LAPTH for its continuous hospitality. This work was supported by the EU Fourth Training Programme "Training and Mobility of Researchers", network "Quantum Chromodynamics and the Deep Structure of Elementary Particles", contract FMRX–CT98–0194 (DG 12 - MIHT).

## A Appendix

In this appendix we identify the origin of the pathological behavior of the cross-section in the vicinity of $E^{\gamma}_{\mathrm{T,min}}$ for symmetric cuts on the photon and jet transverse energies (see Fig. 2). Our aim is to isolate only the leading behavior, i.e. we work in the double logarithmic approximation and drop subleading contributions.

We consider the subprocess $p_1+p_2 \to p_\gamma+p_4+p_5$ where $p_5$ is the momentum of a gluon. This gluon represents a NLO correction to the Born subprocess $p_1+p_2 \to p_\gamma+p_4$ and in the soft approximation ($|\boldsymbol{p}_5| \ll |\boldsymbol{p}_\gamma|$) this NLO correction can be written as

$$\sigma^{\mathrm{NLO}} \sim \int \mathrm{d}\phi_5 \mathrm{d}p_{\mathrm{T}5} p_{\mathrm{T}5}^{-1-2\epsilon} \ln\left(\frac{p_{\mathrm{T}\gamma}}{p_{\mathrm{T}5}}\right) \times \sigma^{\mathrm{Born}}(p_1+p_2 \to p_\gamma + p_4). \quad (9)$$

The cut $E^{\mathrm{jet}}_{\mathrm{T,min}} \le E^{\mathrm{jet}}_{\mathrm{T}}$ ($\equiv p_{\mathrm{T}4}$ in the approximation we consider here) restricts the gluon phase space to values of $p_{\mathrm{T}5}$ smaller than $p_{\mathrm{T}\gamma}$ and depending on $\phi_5$: $p_{\mathrm{T}5}^{\max} = \overline{p}_{\mathrm{T}5}(\phi_5)$. For $E^{\mathrm{jet}}_{\mathrm{T,min}} \le p_{\mathrm{T}\gamma}$ we obtain

$$\sigma^{\mathrm{NLO}} \sim \sigma^{\mathrm{Born}} \int_0^{2\pi} \mathrm{d}\phi_5 \left(\frac{1}{4\epsilon^2} - \frac{1}{2}\ln^2\frac{p_{\mathrm{T}\gamma}}{\overline{p}_{\mathrm{T}5}}\right). \quad (10)$$

The $1/\epsilon^2$ term is cancelled by the virtual contribution. The $\phi_5$ integration is not straightforward because the constraint $E^{\mathrm{jet}}_{\mathrm{T,min}} \le p_{\mathrm{T}4}$ does not lead to a simple expression of $\overline{p}_{\mathrm{T}5}(\phi_5)$, but when $E^{\mathrm{jet}}_{\mathrm{T,min}}$ is close to $p_{\mathrm{T}\gamma}$ we get

$$\sigma^{\mathrm{NLO}} \sim \sigma^{\mathrm{Born}} \times \left(-\frac{1}{2}\ln^2\frac{p_{\mathrm{T}\gamma}}{p_{\mathrm{T}\gamma} - E^{\mathrm{jet}}_{\mathrm{T,min}}}\right). \quad (11)$$

When $E^{\mathrm{jet}}_{\mathrm{T,min}} > p_{\mathrm{T}\gamma}$ we obtain

$$\sigma^{\mathrm{NLO}} \sim \sigma^{\mathrm{Born}} \times \left(\frac{1}{2}\ln^2\frac{p_{\mathrm{T}\gamma}}{E^{\mathrm{jet}}_{\mathrm{T,min}} - p_{\mathrm{T}\gamma}}\right). \quad (12)$$

The cross-section displayed in Fig. 2 is integrated over $p_{\mathrm{T}\gamma}$ from a lower limit $p^{\gamma}_{\mathrm{T,min}}$ to $p_{\mathrm{T}\gamma} = s^{1/2}$. Therefore the soft NLO contribution to the cross-section for $E^{\mathrm{jet}}_{\mathrm{T,min}} < p_{\mathrm{T}\gamma}$ is

$$-\frac{1}{2}\int_{p^{\gamma}_{\mathrm{T,min}}}^{\sqrt{s}} \mathrm{d}p_{\mathrm{T}\gamma}\sigma^{\mathrm{Born}}(p_{\mathrm{T}\gamma})\ln^2\left(\frac{p_{\mathrm{T}\gamma}}{p_{\mathrm{T}\gamma} - E^{\mathrm{jet}}_{\mathrm{T,min}}}\right) \quad (13)$$

$$\approx -\frac{1}{2}\frac{\overline{\sigma}}{(E^{\mathrm{jet}}_{\mathrm{T,min}})^{n_{\mathrm{eff}}-1}} \int_0^{\frac{E^{\mathrm{jet}}_{\mathrm{T,min}}}{p^{\gamma}_{\mathrm{T,min}}}} \mathrm{d}u u^{n_{\mathrm{eff}}-2}\ln^2(1-u),$$

where we used the approximation $\sigma^{\mathrm{Born}} \approx \overline{\sigma}(p_{\mathrm{T}\gamma})^{-n_{\mathrm{eff}}}$ ($n_{\mathrm{eff}} \approx 3$). When $E^{\mathrm{jet}}_{\mathrm{T,min}}$ increases up to $p^{\gamma}_{\mathrm{T,min}}$, the negative contribution (13) to the cross-section becomes more and more dominant and explains the behavior of the cross-section in the range $E^{\mathrm{jet}}_{\mathrm{T,min}} \le p^{\gamma}_{\mathrm{T,min}}$. When $E^{\mathrm{jet}}_{\mathrm{T,min}} > p^{\gamma}_{\mathrm{T,min}}$, the integral over $p_{\mathrm{T}\gamma}$ splits into two parts

$$\int_{p^{\gamma}_{\mathrm{T,min}}}^{\sqrt{s}} \mathrm{d}p_{\mathrm{T}\gamma} = \int_{p^{\gamma}_{\mathrm{T,min}}}^{E^{\mathrm{jet}}_{\mathrm{T,min}}} \mathrm{d}p_{\mathrm{T}\gamma} + \int_{E^{\mathrm{jet}}_{\mathrm{T,min}}}^{\sqrt{s}} \mathrm{d}p_{\mathrm{T}\gamma},$$

the second part being calculated already in (13). The first integral is a positive contribution to the NLO cross-section, given by an expression similar to (13):

$$\frac{1}{2}\frac{\overline{\sigma}}{(E^{\mathrm{jet}}_{\mathrm{T,min}})^{n_{\mathrm{eff}}-1}} \int_1^{\frac{E^{\mathrm{jet}}_{\mathrm{T,min}}}{p^{\gamma}_{\mathrm{T,min}}}} \mathrm{d}u u^{n_{\mathrm{eff}}-2}\ln^2(u-1).$$

This positive contribution explains the behavior of the cross-section for $E^{\mathrm{jet}}_{\mathrm{T,min}} > p^{\gamma}_{\mathrm{T,min}}$.

## References

1. J. Breitweg et al. [ZEUS Collaboration], Phys. Lett. B **472**, 175 (2000) [hep-ex/9910045]
2. L.E. Gordon, W. Vogelsang, Phys. Rev. D **52**, 58 (1995)
3. M. Krawczyk, A. Zembrzuski, hep-ph/9810253; hep-ph/0105166
4. M. Fontannaz, J.P. Guillet, G. Heinrich, Eur. Phys. J. C **21**, 303 (2001) [hep-ph/0105121]
5. J. Breitweg et al. [ZEUS Collaboration], Phys. Lett. B **413**, 201 (1997) [hep-ex/9708038]
6. L.E. Gordon, Phys. Rev. D **57**, 235 (1998) [hep-ph/9707464]
7. M. Fontannaz, D. Schiff, Nucl. Phys. B **132**, 457 (1978)
8. J. Huston, E. Kovacs, S. Kuhlmann, H.L. Lai, J.F. Owens, W.K. Tung, Phys. Rev. D **51**, 6139 (1995) [hep-ph/9501230]
9. L. Apanasevich et al. [Fermilab E706 Collaboration], Phys. Rev. Lett. **81**, 2642 (1998) [hep-ex/9711017]
10. L. Apanasevich et al., Phys. Rev. D **59**, 074007 (1999) [hep-ph/9808467]; L. Apanasevich et al., Phys. Rev. D **63**, 014009 (2001) [hep-ph/0007191]
11. H. Lai, H. Li, Phys. Rev. D **58**, 114020 (1998) [hep-ph/9802414]
12. M.A. Kimber, A.D. Martin, M.G. Ryskin, Eur. Phys. J. C **12**, 655 (2000) [hep-ph/9911379]
13. N. Kidonakis, J.F. Owens, Phys. Rev. D **61**, 094004 (2000) [hep-ph/9912388]
14. E. Laenen, G. Sterman, W. Vogelsang, Phys. Rev. Lett. **84**, 4296 (2000) [hep-ph/0002078]; Phys. Rev. D **63**, 114018 (2001) [hep-ph/0010080]
15. P. Aurenche, M. Fontannaz, J.Ph. Guillet, B. Kniehl, E. Pilon, M. Werlen, Eur. Phys. J. C **9**, 107 (1999) [hep-ph/9811382]
16. P. Aurenche, M. Fontannaz, J.Ph. Guillet, B.A. Kniehl, M. Werlen, Eur. Phys. J. C **13**, 347 (2000) [hep-ph/9910252]
17. J. Binnewies, B.A. Kniehl, G. Kramer, Z. Phys. C **65**, 471 (1995) [hep-ph/9407347]; Phys. Rev. D **52**, 4947 (1995) [hep-ph/9503464]

18. B.A. Kniehl, G. Kramer, B. Pötter, Nucl. Phys. B **582**, 514 (2000) [hep-ph/0010289]
19. J.Ph. Guillet et al., in preparation
20. S. Chekanov et al. [ZEUS Collaboration], Phys. Lett. B **511**, 19 (2001) [hep-ex/0104001]
21. T. Sjostrand, P. Eden, C. Friberg, L. Lonnblad, G. Miu, S. Mrenna, E. Norrbin, Comput. Phys. Commun. **135**, 238 (2001) [hep-ph/0010017]
22. G. Marchesini, B.R. Webber, G. Abbiendi, I.G. Knowles, M.H. Seymour, L. Stanco, Comput. Phys. Commun. **67**, 465 (1992)
23. T. Binoth, J.Ph. Guillet, E. Pilon, M. Werlen, Eur. Phys. J. C **16**, 311 (2000) [hep-ph/9911340]
24. P. Aurenche, A. Douiri, R. Baier, M. Fontannaz, D. Schiff, Z. Phys. C **24**, 309 (1984)
25. R.K. Ellis, J.C. Sexton, Nucl. Phys. B **269**, 445 (1986)
26. P. Aurenche, R. Baier, A. Douiri, M. Fontannaz, D. Schiff, Nucl. Phys. B **286**, 553 (1987)
27. M. Fontannaz, D. Schiff, Z. Phys. C **14**, 151 (1982)
28. P. Aurenche, P. Chiappetta, M. Fontannaz, J.Ph. Guillet, E. Pilon, Z. Phys. C **56**, 589 (1992)
29. S. Catani, Y.L. Dokshitzer, M.H. Seymour, B.R. Webber, Nucl. Phys. B **406**, 187 (1993); S.D. Ellis, D.E. Soper, Phys. Rev. D **48**, 3160 (1993) [hep-ph/9305266]
30. A.D. Martin, R.G. Roberts, W.J. Stirling, R.S. Thorne, Eur. Phys. J. C **14**, 133 (2000)
31. P. Aurenche, J.Ph. Guillet, M. Fontannaz, Z. Phys. C **64**, 621 (1994)
32. L. Bourhis, M. Fontannaz, J.Ph. Guillet, Eur. Phys. J. C **2**, 529 (1998)
33. S. Catani, B.R. Webber, JHEP **9710**, 005 (1997) [hep-ph/9710333]
34. S. Catani, M. Fontannaz, E. Pilon, Phys. Rev. D **58**, 094025 (1998) [hep-ph/9803475]
35. S. Catani, M. Fontannaz, J.Ph. Guillet, E. Pilon, in preparation
36. P. Aurenche, Talk given at the International Conference on the Structure and the Interactions of the Photon (Photon 97), Egmond aan Zee, The Netherlands, 10–15 May 1997 [hep-ph/9706386]
37. S. Frixione, G. Ridolfi, Nucl. Phys. B **507**, 315 (1997) [hep-ph/9707345]
38. P. Aurenche, L. Bourhis, M. Fontannaz, J.Ph. Guillet, Eur. Phys. J. C **17**, 413 (2000) [hep-ph/0006011]